Geophysical Journal International

Geophys. J. Int. (2011) **184,** 12–28 doi: 10.1111/j.1365-246X.2010.04834.x

Structural architecture of oceanic plateau subduction offshore Eastern Java and the potential implications for geohazards

A. Shulgin,[1] H. Kopp,[1] C. Mueller,[2] L. Planert,[1] E. Lueschen,[2] E. R. Flueh[1] and Y. Djajadihardja[3]

[1]*IFM-GEOMAR, Leibniz Institute of Marine Sciences, Wischhofstr.* 1-3, 24148 *Kiel, Germany. E-mail: ashulgin@ifm-geomar.de*
[2]*Federal Institute for Geosciences and Natural Resources (BGR), Stilleweg* 2, 30655 *Hannover, Germany*
[3]*Agency for the Assessment and Application of Technology (BPPT), Jl.M.H. Thamrin No.* 8, *Jakarta* 10340, *Indonesia*

Accepted 2010 September 29. Received 2010 September 27; in original form 2010 April 26

SUMMARY

The region offshore Eastern Java represents one of the few places where the early stage of oceanic plateau subduction is occurring. We study the little investigated Roo Rise oceanic plateau on the Indian plate, subducting beneath Eurasia. The presence of the abnormal bathymetric features entering the trench has a strong effect on the evolution of the subduction system, and causes additional challenges on the assessment of geohazard risks. We present integrated results of a refraction/wide-angle reflection tomography, gravity modelling, and multichannel reflection seismic imaging using data acquired in 2006 south of Java near 113°E. The composite structural model reveals the previously unresolved deep geometry of the oceanic plateau and the subduction zone. The oceanic plateau crust is on average 15 km thick and covers an area of about 100 000 km^2. Within our profile the Roo Rise crustal thickness ranges between 18 and 12 km. The upper oceanic crust shows high degree of fracturing, suggesting heavy faulting. The forearc crust has an average thickness of 14 km, with a sharp increase to 33 km towards Java, as revealed by gravity modelling. The complex geometry of the backstop suggests two possible models for the structural formation within this segment of the margin: either accumulation of the Roo Rise crustal fragments above the backstop or alternatively uplift of the backstop caused by basal accumulation of crustal fragments. The subducting plateau is affecting the stress field within the accretionary complex and the backstop edge, which favours the initiation of large, potentially tsunamogenic earthquakes such as the 1994 $M_w = 7.8$ tsunamogenic event.

Keywords: Tomography; Subduction zone processes; Oceanic plateaus and microcontinents; Crustal structure; Asia.

1 INTRODUCTION

The converging margins around the world are major areas for generating the most devastating earthquakes and tsunamis. Any variations in the subduction systems are of extreme importance due to the changes in the geohazards situation. In this work we investigate the subduction of a previously little investigated oceanic plateau—the Roo Rise, its structure and its interaction with the Java margin at around 113°E. We focus on the recovery of the structural architecture in the region and its tectonic interpretation. We provide insights on the following questions for this particular region: (1) what are the effects of an oceanic plateau subduction, (2) what consequences does the subducting plateau have on the forearc deformation, (3) what is the structure of the forearc in such settings and (4) what are the effects that the subducting plateau have on the earthquake and tsunami generation?

The Sunda arc forms a part of more than 5000-km-long continuous subduction system, spanning from Flores and Sumba islands in the east to Burma in the northwest. The transition from the Sunda arc to the Banda arc is located at around 121°E, where the Australian continental shelf is approaching the trench (Shulgin *et al.* 2009). Both arcs are active since the Eocene collision of India and the Sundaland (the continental core of the southeast Asia (Hamilton 1988; Hall 2002; Hall & Smyth 2008) and are formed by the subduction of the Indo-Australian Plate underneath Eurasia (Hamilton 1979). The basement underneath Eastern Java is formed by arc and ophiolithic rocks accreted during the Mesozoic (Hall & Smyth 2008). Based on zircon dating, Smyth *et al.* (2007) propose an Archean continental fragment of Australian origin to be trapped between the forearc and the present volcanic arc in Eastern Java. The current convergence rate offshore Western Java is estimated to be 6.7 ± 0.7 cm yr^{-1} in the direction 11°N that is almost perpendicular to the trench (DeMets

et al. 1994; Tregoning *et al.* 1994). A northward shift of the volcanic arc is recognized in Eastern Java with the present-day arc located *ca*. 50 km to the north of an older currently inactive volcanic arc (Hall & Smyth 2008); the shift is associated with changes in the subduction setting and interaction with the proposed Gondwana revenue (Smyth *et al.* 2007).

The Roo Rise oceanic plateau is located offshore Eastern Java. Oceanic plateaus are defined as a large, relatively flat submarine region that rises well above the level of the ambient seabed [*Encyclopedia Britannica*]. Oceanic plateaus can be formed from the remnants of continental crust or be a part of marine large igneous provinces. Currently there are no definitions based on the crustal structure. Their presence at the subduction zones is crucial in the evolution and dynamics of convergent margins. The subduction of the oceanic plateau triggers qualitatively different processes in the subduction system as compared to the subduction of 'normal' oceanic crust (White *et al.* 1992). The major differences caused by the approach of elevated rough bathymetric features (sea plateau, seamounts) to the trench include active frontal erosion of the margin, uneven uplift and deformation of the forearc, and a principally different regime of seismicity (Yamazaki and Okamura, 1989; Scholz & Small 1997). The migration of the trench is also in a good agreement with the numerical modelling of oceanic plateau subduction, comparable to the subduction of the Roo Rise (Gerya *et al.* 2009; Mason *et al.* 2010).

A 135-Ma-old Indian oceanic crust is currently subducting offshore Central–Eastern Java (Moore *et al.* 1980; Masson 1991) in the vicinity of the Roo Rise oceanic plateau. The Roo Rise is a broad smooth bathymetric feature with a number of isolated summits with an average elevation of about 2000 m above the adjacent oceanic floor (Fig. 1). It forms the eastern extension of the Christmas Island Seamount Province (Fig. 1). Planert *et al.* (2010) determine a crustal thickness of 10 km and show that earlier estimates by Curray *et al.* (1977) may be regarded as a lower limit. Rock samples taken across the entire Christmas Island Seamount Province do not show any clear formation time trend across the region (Werner *et al.* 2009). Based on dredged samples (dredging location closest to the study area is shown in Fig. 1), the Roo Rise is composed of strongly altered olivine phyric lava fragments with Mn-crusts and sediment. The formation of the plateau is associated with a series of large magmatic events as no formation time trend is observed. The increased crustal thickness should be accommodated by thickening of the gabbroic or basaltic layer (van Hunen *et al.* 2002). In order to explain the absence of a correlated gravity anomaly, the presence of a low density compensating crustal root was suggested (Newcomb & McCann 1987). Currently, the northern flank of the Roo Rise enters the trench (Fig. 1). Based on the bathymetry the edge of the plateau, which already subducted could be located as far as 70 km north from the trench, implying that it started to subduct 1.1–1.3 Ma. However, there is no direct evidence.

Offshore Central–Eastern Java, where the northern portion of the Roo Rise has already started to subduct, a northward displacement of the trench by 40 km on average is observed; the subduction of the individual seamounts causes an additional landward retreat of the deformation front by up to 10 km (Kopp *et al.* 2006). The bathymetric data collected in the trench area around 113°E (Fig. 1) show the trench is mostly devoid of sediments, except for local ponded accumulations associated with original seafloor fabric (Planert *et al.* 2010). Similar observations have been reported for the trench segment in between 108°E and 114°E (Curray *et al.* 1977; Masson *et al.* 1990). This study is a part of a large scale effort where data along the margin from Java to Lombok have been collected and analysed, for details on the adjacent profiles please see Planert *et al.* (2010), Shulgin *et al.* (2009) and Lueschen *et al.* (2010). These profiles augment earlier work on the Sumatra and Sunda Strait and Western Java (Kopp *et al.* 2002), so that we are able to describe the entire Sunda Arc subduction zone.

The forearc high, characterized in this area by a number of isolated well-defined peaks, shows an average elevation of *ca*. 800–1200 m, contrasting with the deeper forearc high ridges to the west (Kopp *et al.* 2001, 2002) and to the east offshore Lombok (Planert *et al.* 2010) (Fig. 1). The location of the forearc high peaks correlates with the proposed locations of completely subducted seamounts; however, the estimated subducted volume is smaller than the observed uplift of the forearc (Masson *et al.* 1990).

A number of tsunamogenic earthquakes have been recorded in the areas of seamount subduction offshore Java, which brings these locations into special focus in terms of geohazards. In 1994 and 2006, magnitude 7.8 earthquakes stroke offshore Java causing more than 1000 deaths due to the triggered tsunamis. Abercrombie *et al.* (2001) showed that the highest slip was collocated with the proposed location of a subducted seamount. More recently, Bilek & Engdahl (2007) and Kopp *et al.* (2009a) enhanced the idea of the correlation of structural forearc highs and associated subducted structures with the maximum slip of tsunami-generating earthquakes. The distribution of shallow earthquakes shows a pronounced spatial clustering, associated with the rough oceanic seafloor (Fig. 1).

2 DATA ACQUISITION AND MODELLING

We present *Vp* seismic tomography models of the Java forearc (Fig. 2, discussed below) (located offshore Eastern Java at 113°E), which are further constrained by gravity modelling. The SINDBAD marine seismic experiment onboard R/V 'Sonne' in 2006 (Fig. 1) included multichannel seismic reflection profiling (MCS) accompanied by gravity measurements, seismic refraction profiling with ocean-bottom seismometers (OBS) and hydrophones (OBH) (Mueller *et al.* 2008) and high-resolution multibeam bathymetry.

2.1 Acquisition

The corridor near 113°E consists of three wide-angle seismic refraction/reflection profiles with collocated MCS data and gravity measurements. Two profiles (P-42 and P-43) run north–south and are joint to one continuous transect, trending approximately perpendicular to the trench (Fig. 1). A total of 46 ocean bottom stations (Bialas & Flueh 1999) were deployed along these profiles. The profiles P-42/P-43 have an overlap of about 75 km, and we will refer to this joint profile as P4–23. P-41 is a shorter, east–west trending, trench parallel line located on the top of the forearc high (Fig. 1). During OBS recording, four G-gun clusters with a total volume of 64 l shot at 210 bar were used as seismic source. The average spacing between the shots is around 150 m; the average instrument spacing is 7 km. For the MCS reflection profiling, shots of ten G-gun clusters fired at 135 bar with the total volume of 56 l at a shot spacing of 50 m were recorded on a 3000 m long 240-channel streamer (Lueschen *et al.* 2010).

2.2 Processing

The processing of the ocean bottom data included the localization of the ocean bottom instruments using the arrival time of the direct

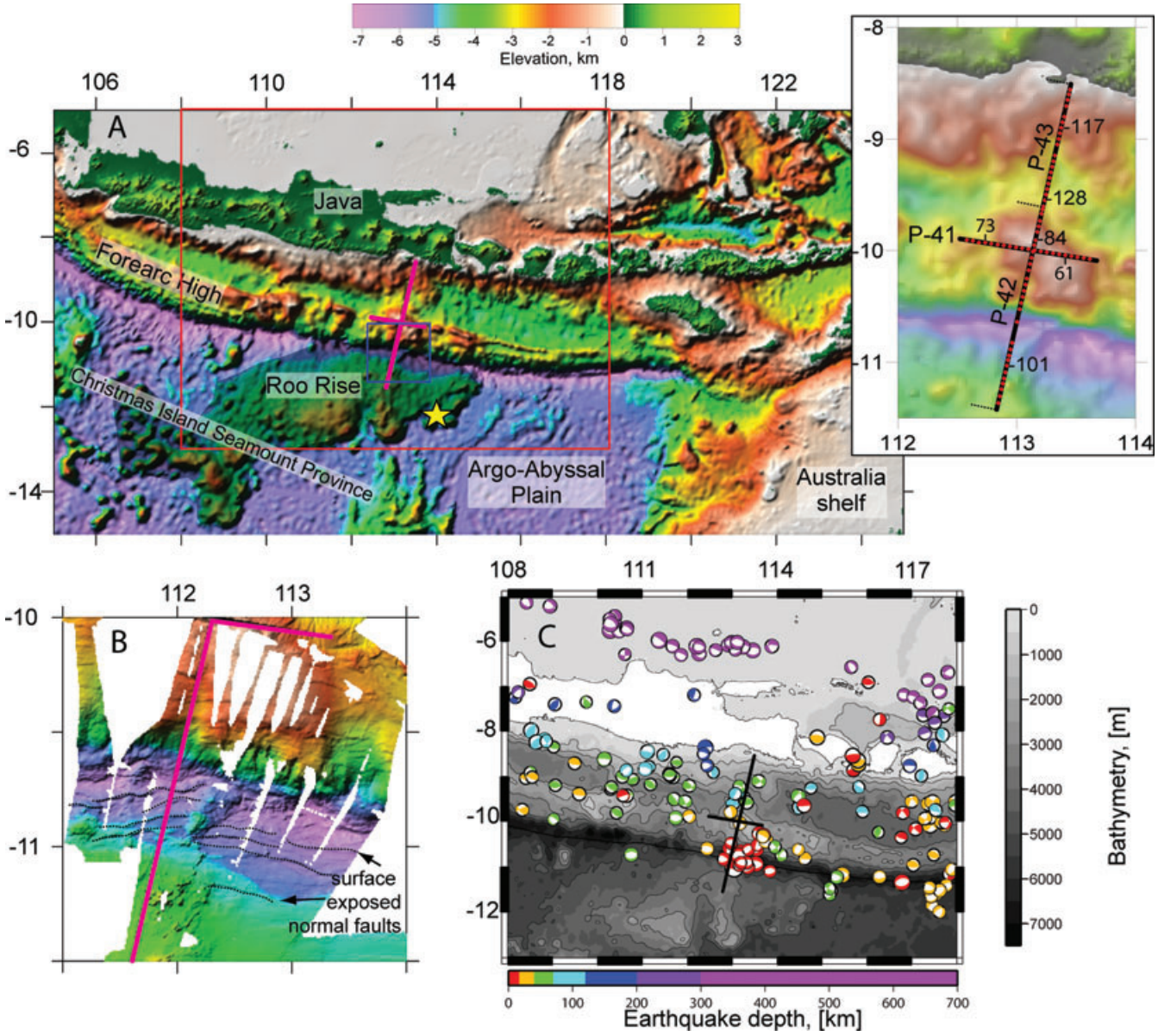

Figure 1. Topographic map of the study area. Seismic profiles examined in this study are shown by magenta lines in panel A and B and with black lines on C plot. Panel (a) shows the global bathymetry/elevation for the area around the Java trench. The insert map at the right shows the detailed geometry of the profiles and the location of ocean bottom stations shown in Figs 3 and 4, overlain on the bathymetry map. The spatial extent of the Roo Rise oceanic plateau is shown with dark shading. Yellow star marks the dredging samples location on Roo Rise (Werner *et al.* 2009). Panel (b) is a close up of the area marked by blue box in A. The multibeam bathymetry data collected during the cruise (the colourscale is identical to A) reveals seamounts and normal faults. Panel (c) shows the earthquake spatial and depth distribution and the focal mechanisms for the area marked by the red box in A (data are taken from the *Harvard Centroid Moment Tensor* catalogue).

water wave and the exact shot point geometry. A time-gated deconvolution was applied to remove predictable bubble reverberations to produce a signal free of the disturbing interference of multiple and primary phases (Wiener 1949). Finally, a time and offset-variant Butterworth filter, in which the pass-band moves towards lower frequencies as record time and offset increase, was applied to consider frequency changes caused by signal attenuation. The processing of the MCS data is described in detail by Lueschen *et al.* (2010).

Data examples are shown in Figs 3 and 4 for profiles P4–23 and P-41, respectively. For line P4–23, the stations located on the oceanic plate south of the trench (instruments 97–107) show clear records of the refracted phases together with clear oceanic Moho reflections (PmP) (Fig. 3a). These stations recorded Pn oceanic mantle phases reaching offsets up to 180 km (Figs 3a and b). The stations placed on top of the accretionary prism and forearc high (instruments 83–96) recorded refracted arrivals within shorter offsets compared to stations deployed on the oceanic crust. Reflections from the top of the oceanic crust (PtocP) were recorded as well as the oceanic Moho reflections (PmP) (Fig. 3b). Clear records of the forearc Moho reflections (PmfP) and the forearc Pnf phases with offsets up to 150 km are seen on the stations deployed along the northern part of the profile (instruments 108–128) (Figs 3c and d). For the trench-parallel profile P-41, the first arrival phases are clearly identified within 50 km offset, together with the reflections from the top of the

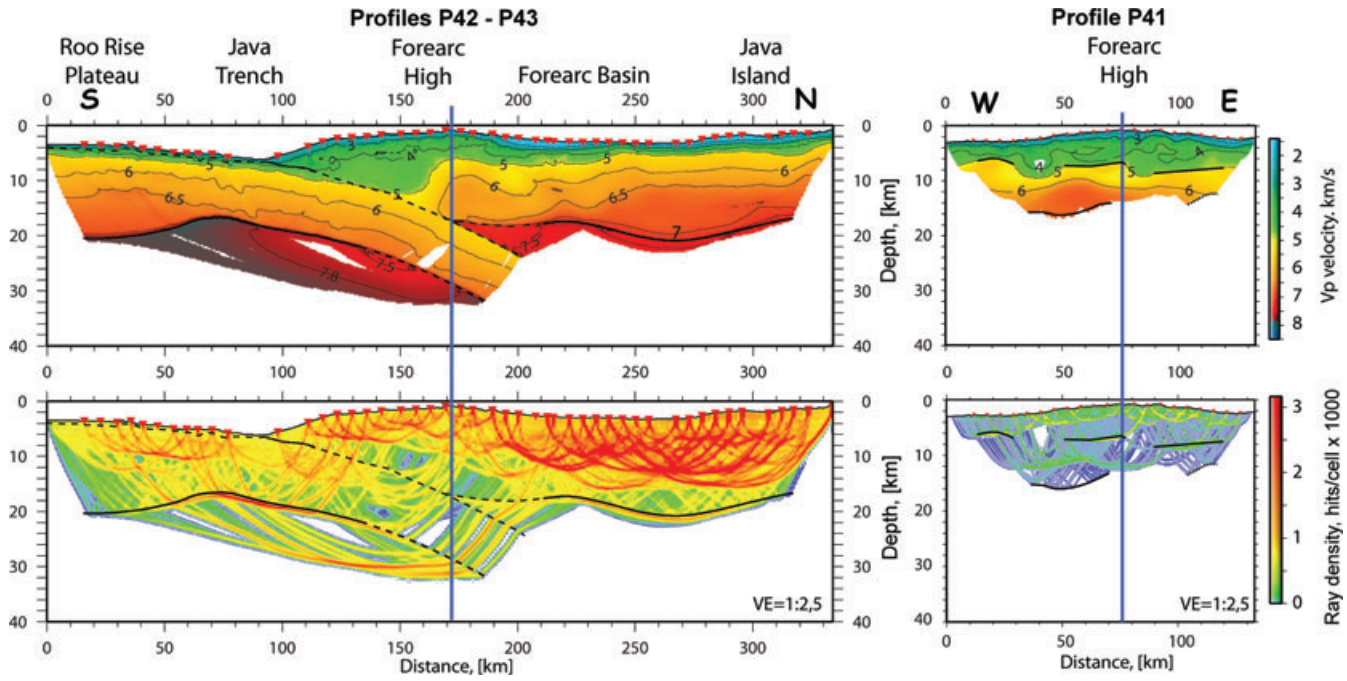

Figure 2. The results of the joint tomographic inversion for the profiles P4–23 and P-41. Top plots show the modelled *Vp* velocity distribution together with the recovered deep reflector geometry. Bottom plots show the seismic ray path density distributions. Both of the profiles are plotted with the identical scales and colourcodes. The solid black lines are the actually recovered positions of the reflectors and the dashed lines are the extrapolated positions based on the velocity distribution, MCS, and gravity models. Vertical blue line shows the cross points of the profiles.

basement (PtfP) (Fig. 4). Several stations (instruments 58–59, 61 and 72–74) on this profile have recorded plate interface reflections (PpintP) (Fig. 4).

2.3 Tomographic inversion

The seismic velocity distribution was modelled by joint refraction/reflection 2-D tomographic inversion (Korenaga *et al.* 2000). We applied a 'top to bottom' approach with a simple layered starting model. The grid spacing was defined by 250 m in the horizontal direction and with vertical spacing increasing with depth from 50 m at the top to 330 m at 40 km depth. The correlation length parameters were chosen to be 1 km × 0.2 km (horizontal × vertical) at the top and linearly increasing with depth to 8 km × 4 km at 40 km depth. Initially, the model was constrained only for the near offsets; then the depth extent of the ray coverage was increased to include the entire model space, with a simultaneous inversion for the reflector positions based on the available reflection phases. 46 stations were available for profile P4–23 with a length of 334 km, resulting in ∼36 500 first arrival traveltime picks and ∼7000 reflected picks. The shorter (135 km long) profile P-41 was covered by 21 stations, summing up to ∼9300 first arrival traveltimes and ∼1200 reflected picks. Data examples are shown in Figs 3 and 4. All available picked traveltimes and the fit of the corresponding computed traveltimes are shown on Fig. S1. The structure of the sediment and the basement topography were adopted from the MCS data (Lueschen *et al.* 2010), thus constraining the upper section of the profiles in great detail. Additionally, the top of the oceanic crust as identified in the depth-migrated MCS data was incorporated into the tomography model. The generalized routing during the inversion was as follows: constraining the interface geometry based on the corresponding MCS depth sections where available; inverting the near offset refracted phases to verify the consistency between data sets; fixing the upper section of the model with a weight of 1000 compared to the deeper sections. Then, we ran the simultaneous inversion for the velocity and reflector geometry for the next depth layer. Subsequently, we fixed the obtained layer structure and repeated the previous step for the following deeper layer. Finally, we kept the entire crustal structure fixed and inverted for the velocity in the upper mantle. The final models for all of the profiles are shown in Fig. 2.

2.4 Resolution tests

Several tests were performed to check the resolution of the obtained models. Initially, we used a forward ray shooting method to compute the synthetic traveltimes for the first arrival and reflected phases through our final models. The comparison of the seismic sections and the synthetic calculated traveltimes for several stations on both of the profiles is shown in Figs 3 and 4. The calculated traveltimes, as predicted by the tomographic *Vp* velocity models, are in a good agreement with the recorded seismic sections. All the refracted phases, including Pg and Pn, are fitted to the observed arrivals. The reflection phases (PmP, PmfP and PtocP) also match the recorded data; however, pre-critical reflections are not clearly identified in the seismic record sections.

Checkerboard resolution tests have been computed for both of the profiles to gain information on the spatial and amplitude resolution, which is dependent on the given ray geometry and the velocity distribution. The final *Vp* velocity model is perturbed by a small (compared to the real) value using a checkerboard pattern (for P4–23 additionally an isolated Gaussian anomaly pattern was used). Synthetic traveltimes are computed through the perturbed medium for the same source–receiver geometry as in the tomographic inversion. Subsequently, the tomography is computed based on the synthetic traveltimes in order to recover the initial perturbation pattern. The results of a test for P4–23 are shown in Figs 5(a)–(c). Three different anomaly sizes were used in the tests: 5 × 2.5 km,

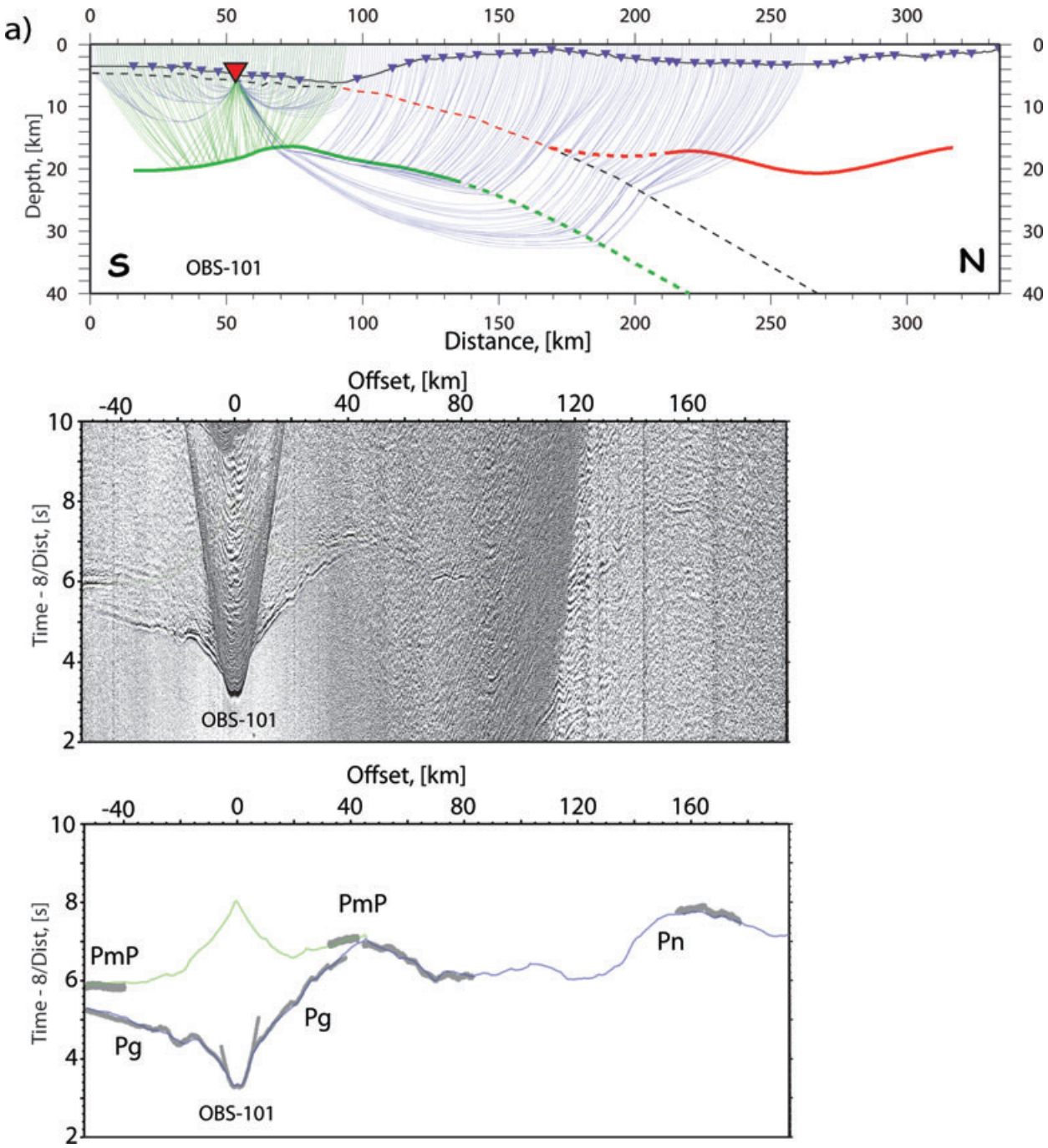

Figure 3. A forward ray shooting test for the selected stations on profile P4–23. For each station the first arriving and reflected traveltimes through the final model were computed and plotted on top of the actual seismic records. Bottom plots show with grey lines the picked phases, with width of the line representing the picking uncertainty. The computed traveltimes through the final model show good fit to the picked phases. Blue line – first arriving phases, green – reflections from the oceanic crust Moho, red – reflections from the forearc crust Moho. Top sections in each of the subplots show the schematic model of the profile. Solid lines correspond to well-defined reflectors constrained by wide-angle seismic data; dashed lines – structural interfaces constrained from MCS and/or gravity data, but purely resolved by the OBS data set. The corresponding ray paths, colourcoded as described above, are shown above each station in the model window.

10 × 5 km and 20 × 10 km (horizontal × vertical size). For all of them the starting model was perturbed using ±5 per cent values. For the small scale perturbation, the model is recovered down to a depth of 12 km, which roughly corresponds to the top of the forearc basement that we define to be around 5 km s^{-1} isocontour (Fig. 5a). The 20 × 10 km size perturbation was adequately recovered down to a 20 km depth, which correlates with the location of the horizontal segments of the oceanic and forearc crust (Fig. 5c). The middle size pattern showed, as expected, an intermediate resolution down to a 16 km depth (Fig. 5b). Portions of the model deeper than ∼20 km failed to be recovered even with the biggest size pattern. To check the model validity for these areas, a resolution test using a single isolated Gaussian anomaly was performed. The anomaly was centred at 130 km offset and at 25 km depth. The tests were performed

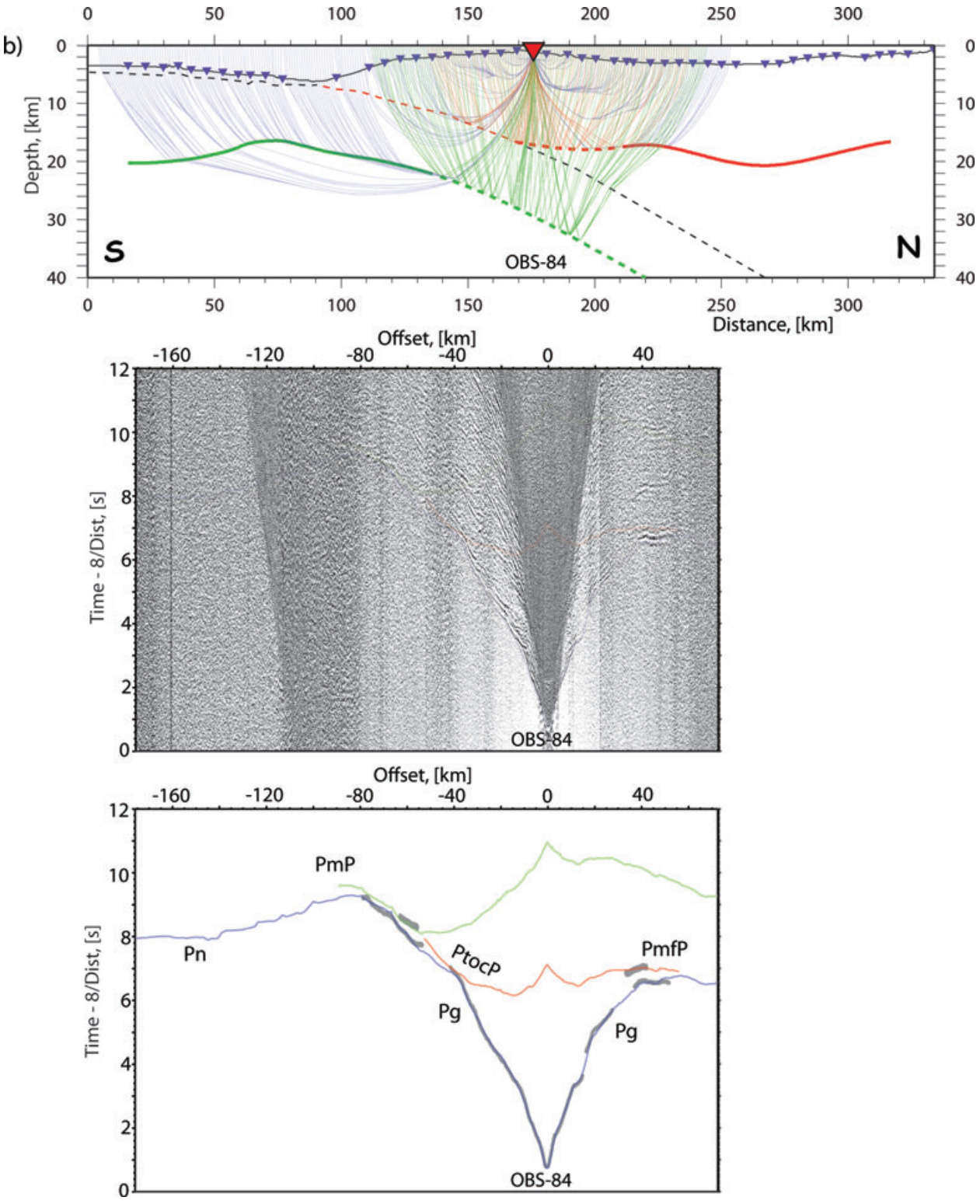

Figure 3. (*Continued.*)

for +10 and –10 per cent anomalies. As displayed in Figs 5(f) and (h), for the negative anomaly it was not possible to recover neither the shape nor the real amplitude of the anomaly due to the geometry of the seismic rays in this area, which are mostly non-crossing. For the positive anomaly test, the amplitudes were recovered; however, the location is smeared along the ray paths. In tomographic inversions with similar geometries (i.e. a small number of crossing rays), it is normal to observe the effect of averaging of the anomaly along the whole ray path between the crossing points. This is the case with the P4–23 profile. Additionally, the structure was checked by fitting the position of the critical distances for PmP reflections, this supports the obtained depth and velocity contrast at Moho (Fig. 6).

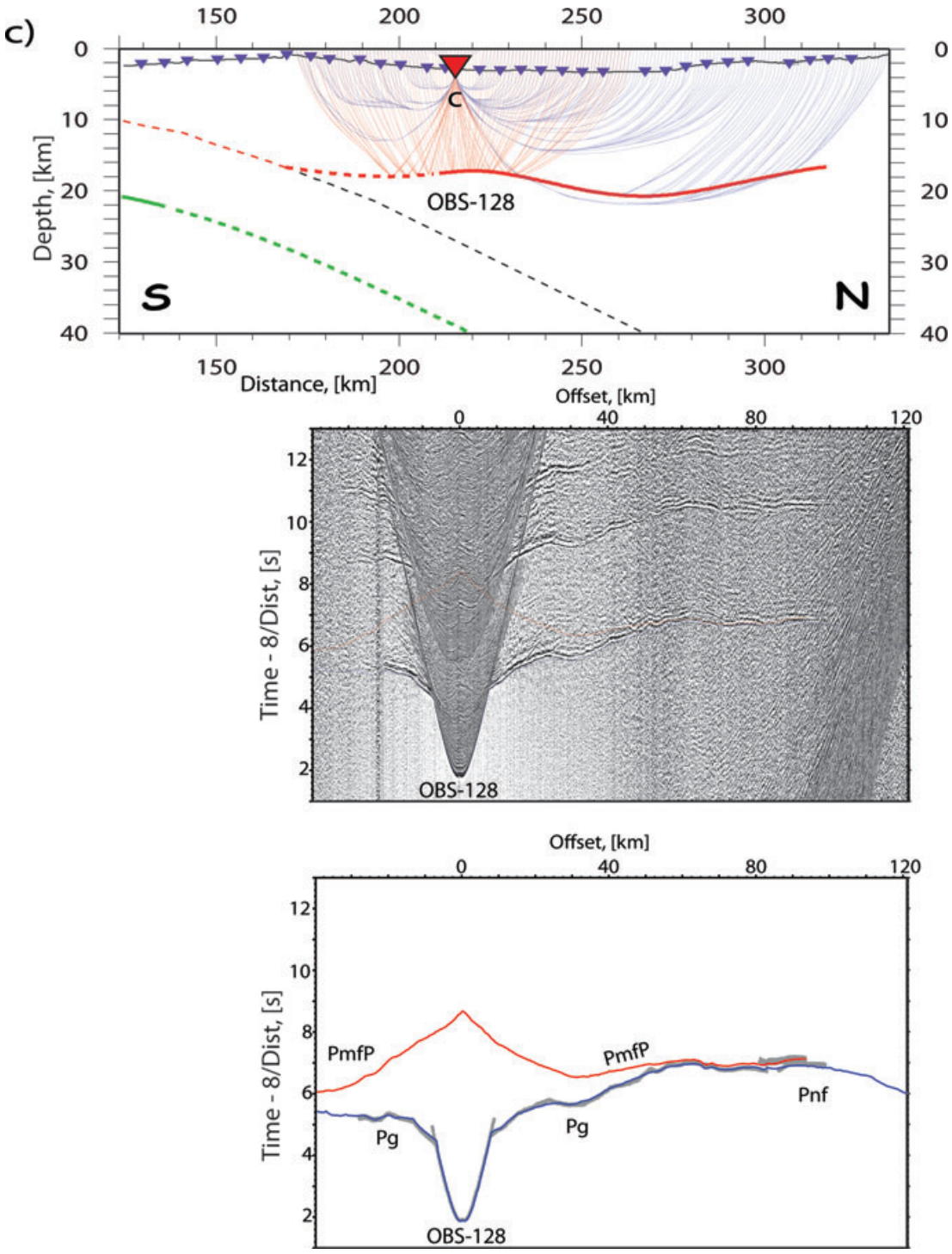

Figure 3. (*Continued.*)

Based on the resolution tests, it is likely that during the tomographic inversion the actual *Vp* velocity values tend to be overestimated and can be in the range of –7 to +3 per cent from the ones recovered for depths greater than 20 km.

Similar to P4–23, checkerboard tests were conducted for profile P-41. The results are shown in Figs 5(d) and (e). Two different pattern sizes were tested: 5 × 2.5 km and 10 × 5 km, both with a ±5 per cent amplitude perturbation. The smaller size anomalies are recovered down to 6 km depth, while the larger ones are recovered down to 12 km depth.

2.5 Gravity modelling

The resulting *Vp* velocity seismic tomography model for profile P4–23 was extended by 100 km both to the north and to the south and down to a depth of 75 km, to be used in forward gravity modelling. Seismic velocities were converted to densities using empirical and experimental relationships (Christensen & Mooney 1995; Carlson & Herrick 1990) and the subducting slab was extended down to 75 km depth, where the deep seismicity is observed. A constant density of 3.30 g cm^{-3} was assumed for the forearc mantle, with

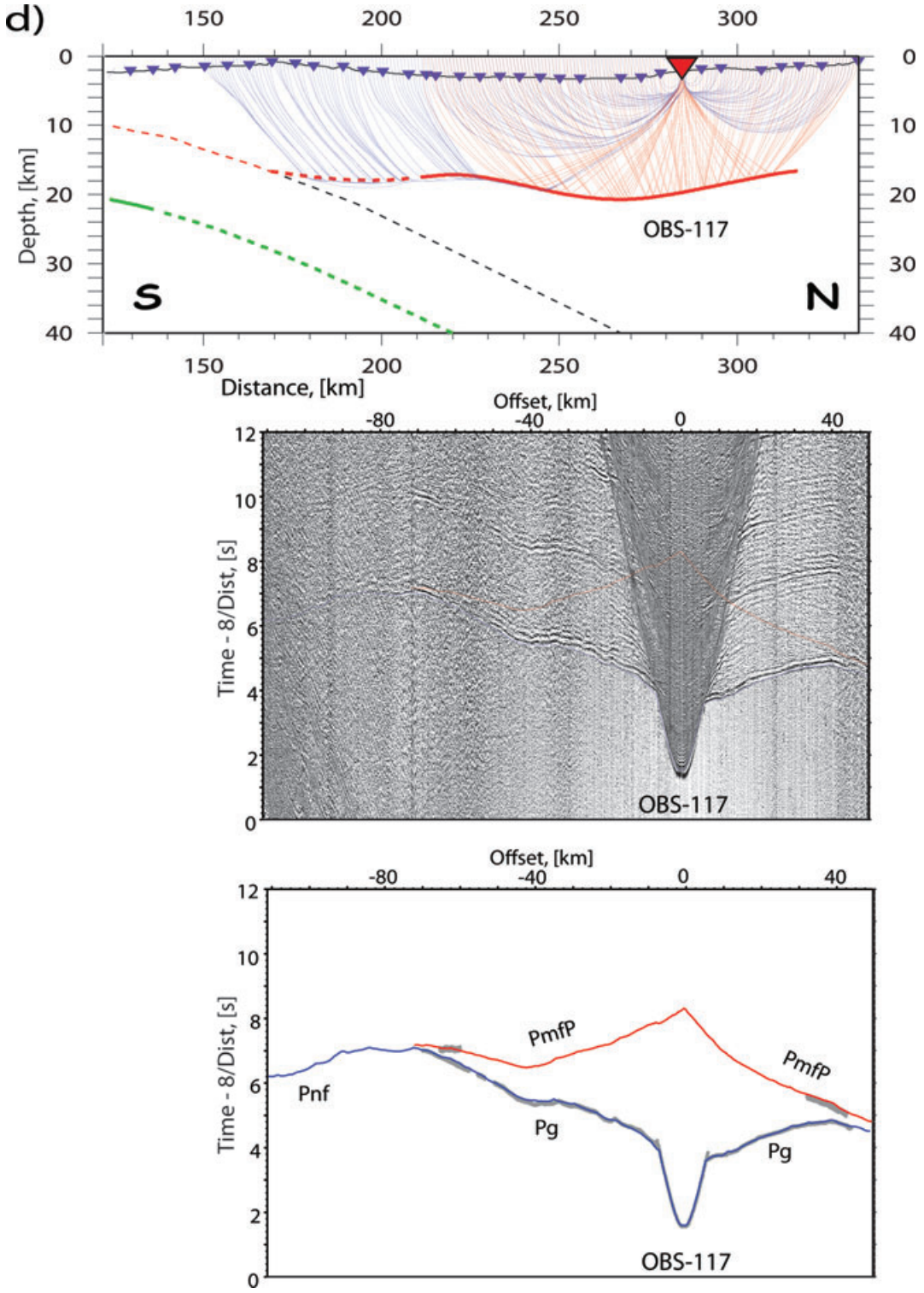

Figure 3. (*Continued.*)

the exception of the 30-km-long innermost mantle wedge where a density of 3.27 g cm^{-3} was used (Fig. 7). The calculated gravity response of the model is in a good agreement with the observed data. The maximum misfit of 15–20 mGal is observed at the edge of the profile.

The area around the profile P4–23 shows a high degree of bathymetric changes in the east–west direction, associated with isolated forearc highs and the extended shelf zone offshore Java to the west of the northern termination of the profile. There is also a possibility for lateral variations of forearc crust offline the profile. Although these features should produce measurable 3-D effects on the gravity field along the profile, their effects were ignored in the gravity modelling. Despite the above mentioned simplifications, the gravity modelling confirms the features resolved by the tomographic

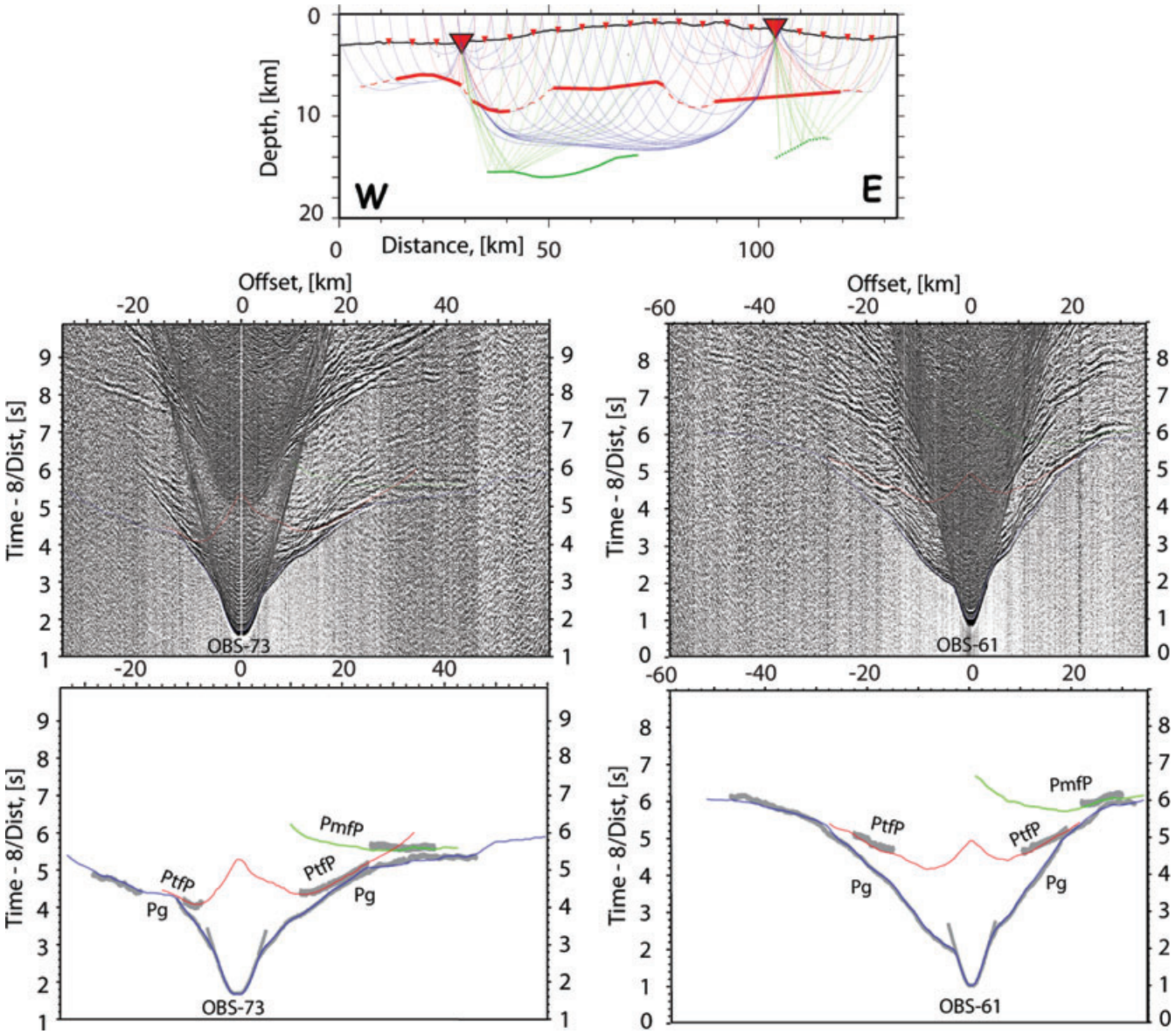

Figure 4. The forward ray shooting test for the selected stations on profile P-41. For each station the first arriving traveltimes (blue lines) through the final model were computed and plotted on top of the actual seismic records. Red and green lines are the synthetic reflection traveltimes from the top of the basement and plate interface, correspondingly. Bottom plots show with grey lines the picked phases, with width of the line representing the picking uncertainty. The top plot shows the locations of the corresponding stations and the ray paths for both stations, colourcoded as described above. Solid lines correspond to the well-defined portions of the reflectors. Dashed lines are reflectors that are purely resolved, or where the strong 3D propagation effects are assumed.

inversion (Fig. 7). The increased crustal thickness of the Roo Rise is required to fit the gravity field. The low mantle velocities, recovered in-between offsets of 60 and 160 km, correlate with the zone of a decreased mantle density of 3.29 g cm^{-3}. Such geometry of the forearc crust and the decreased density in the forearc mantle, associated with a relatively slow velocity in the forearc mantle, are required to fit the gravity data. Additionally, the possibility for the near vertical backstop, as seen offshore Lombok (Planert *et al.* 2010) has been tested (Fig. 7). The larger misfit with the observed gravity, compared to dipping backstop, further supports that the study area is transitional from Lombok domain to Java domain.

3 RESULTS AND DISCUSSION

The results are discussed from south to north of the region, starting from the southern segment of profile P4–23 towards Java. They are based on the joint interpretation of the wide-angle reflection/refraction tomography models, MCS data, and gravity model shown in Figs 2, 7, 8 and 9.

3.1 Roo Rise crustal structure

The southernmost section from 0 to 65 km offset on the north-south striking profile (P4–23) is the area where the Roo Rise oceanic

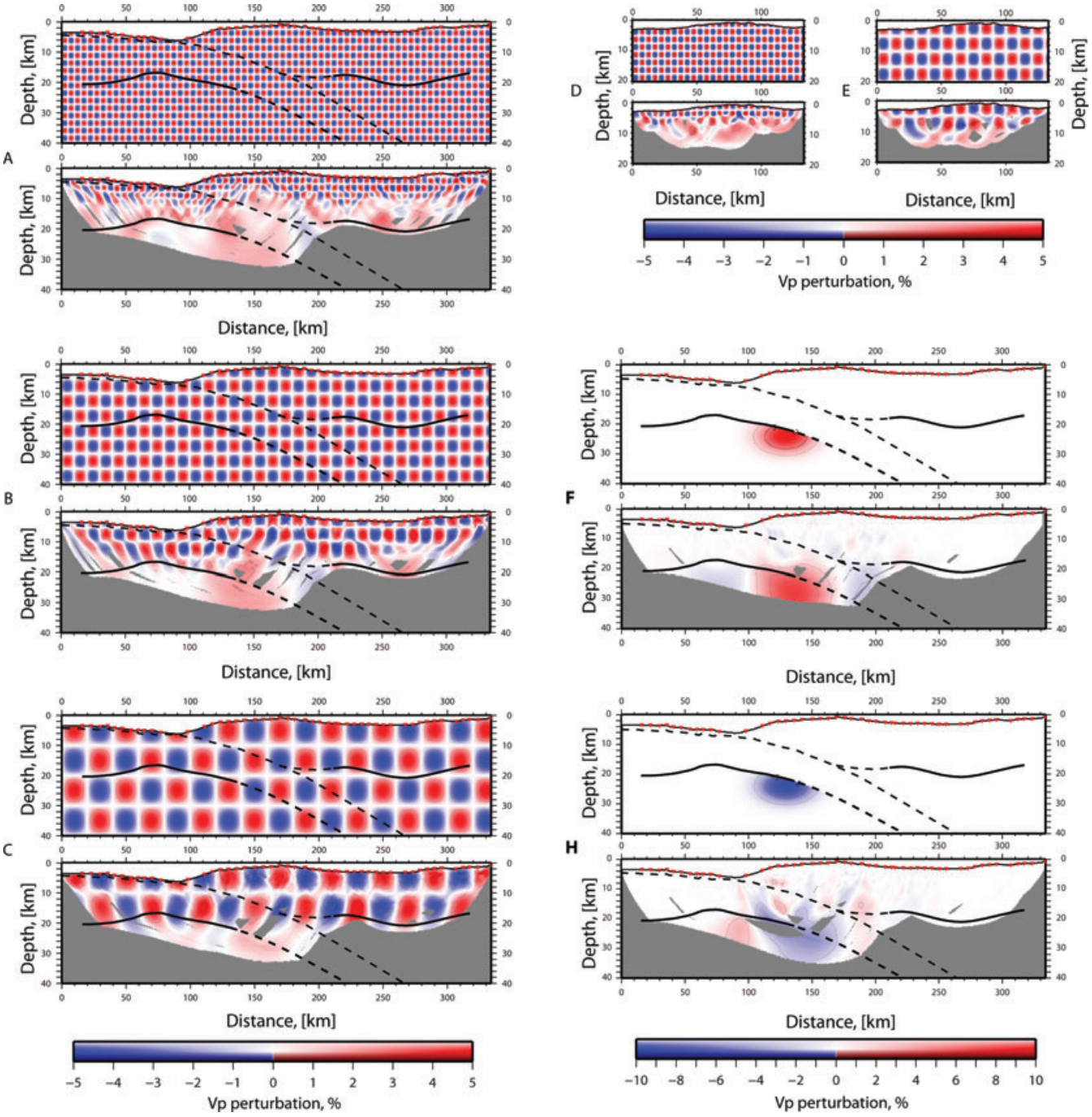

Figure 5. The results of the resolution tests. For each of the subplots the top figure is the synthetic resolution pattern and the bottom one is the recovery. A, B and C are the ±5 per cent *Vp* anomaly tests for profile P4–23. The sizes of the anomalies are: (A) 5 × 2.5 km; (B) 10 × 5 km; (C) 20 × 10 km (first number – horizontal extend, second – vertical). (D) and (E) are the ±5 per cent *Vp* anomaly tests for profile P41. The sizes of the anomalies are: (D): 5×2.5 km; (E) 10 × 5 km; (first number – horizontal extend, second – vertical). F and H are the resolution tests for profile P4–23 with a single isolated anomaly (F: +10 per cent; H: –10 per cent). Black solid and dashed lines are structural elements, the same as in Fig. 2.

plateau enters the trench (Fig. 2). The water depth is increasing here from 3 km at the southern end of the profile in the oceanic domain to 6 km depth at the trench. The *Vp* velocity structure of the upper portion of the oceanic plate is laterally homogeneous: velocities increase from about 2.7 to 3.0 km s^{-1} below the seafloor (bsf) to 5 km ;s^{-1} at about 2 km depth bsf (Fig. 8). At greater depth, the velocity gradient decreases and the velocities rise to 6.5–6.8 km s^{-1} at the Moho which is located at 20–16 km depth (Fig. 2). Thus, the crustal thickness of the plateau varies from 18 km to 11 km (Fig. 2); these values are significantly greater than predicted earlier (Curray *et al.* 1977). The position of the critical distance for the PmP reflections (Fig. 6) fits the data, confirming the velocity model and the oceanic Moho topography. As is seen in the velocity model (Fig. 2), the major increase of the crustal thickness is accommodated by thickening of the lower oceanic crust. The gravity modelling of this crustal block yields a reasonable fit to the observed gravity field, which confirms the thickened (up to 20 km) crust underneath the oceanic plateau (Fig. 7). This result confirms the suggestion of

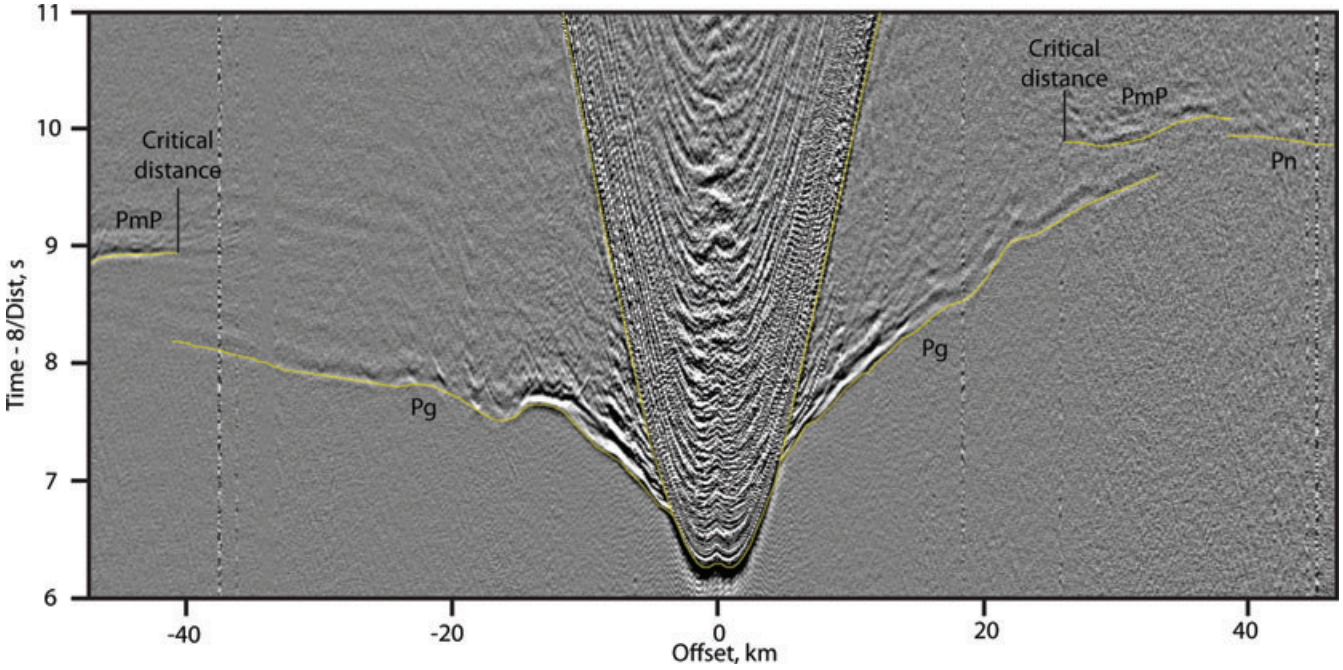

Figure 6. Record section of the vertical component of the OBH-101 located on the P4–23 profile around 51 km offset. Yellow lines show some selected phases. The forward ray shooting method nicely fits the observed critical points for the PmP.

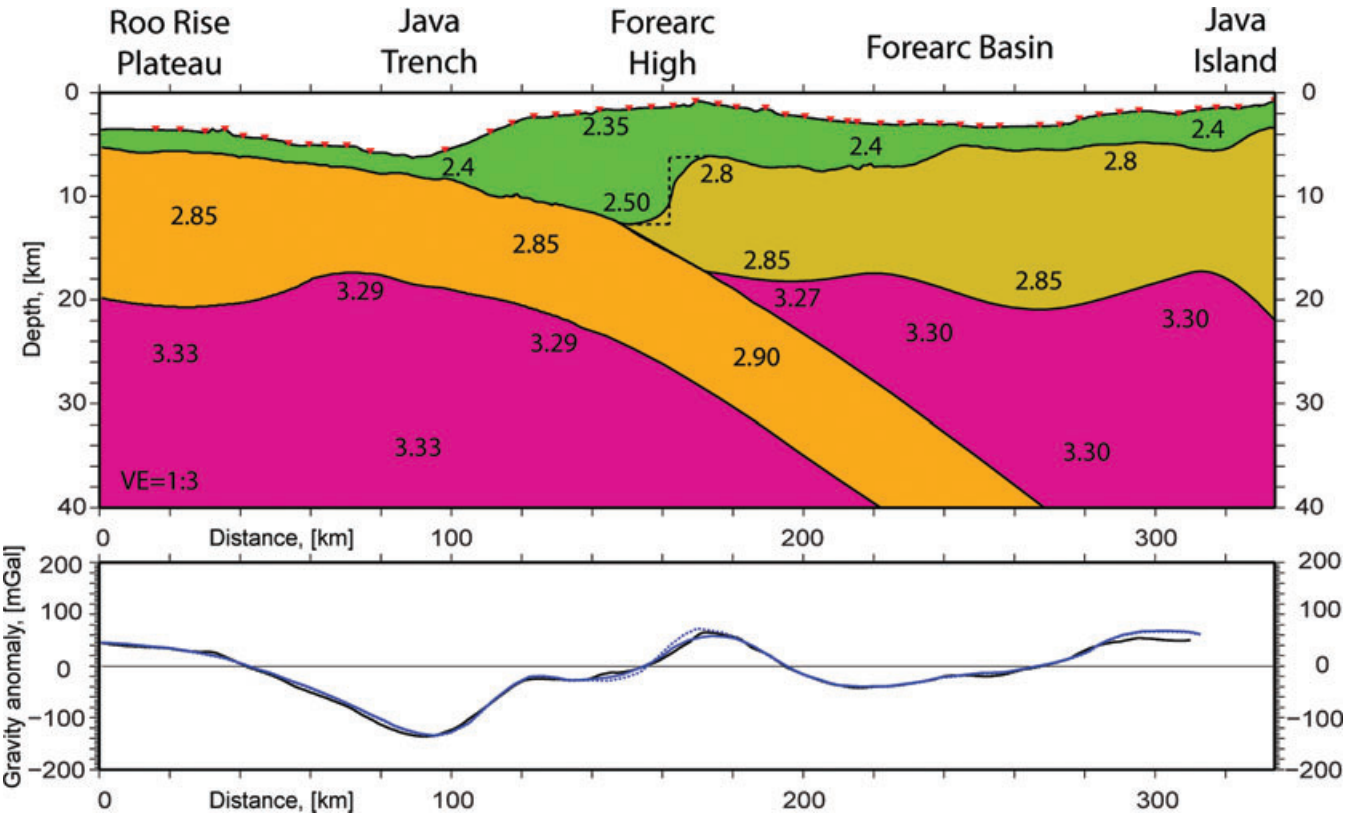

Figure 7. The gravity model for the profile P4–23. Top plot shows the density distribution in the model. Numbers correspond to the density values in units of g cm^{-3}. Densities below the shown depth are kept constant. The bottom plot shows the observed (black) and calculated (blue) free-air gravity anomalies along the profile. The dashed line on top plot corresponds to the gravity model where the backstop is assumed to be pure vertical; the computed gravity anomaly is shown on the bottom plot by dashed blue line.

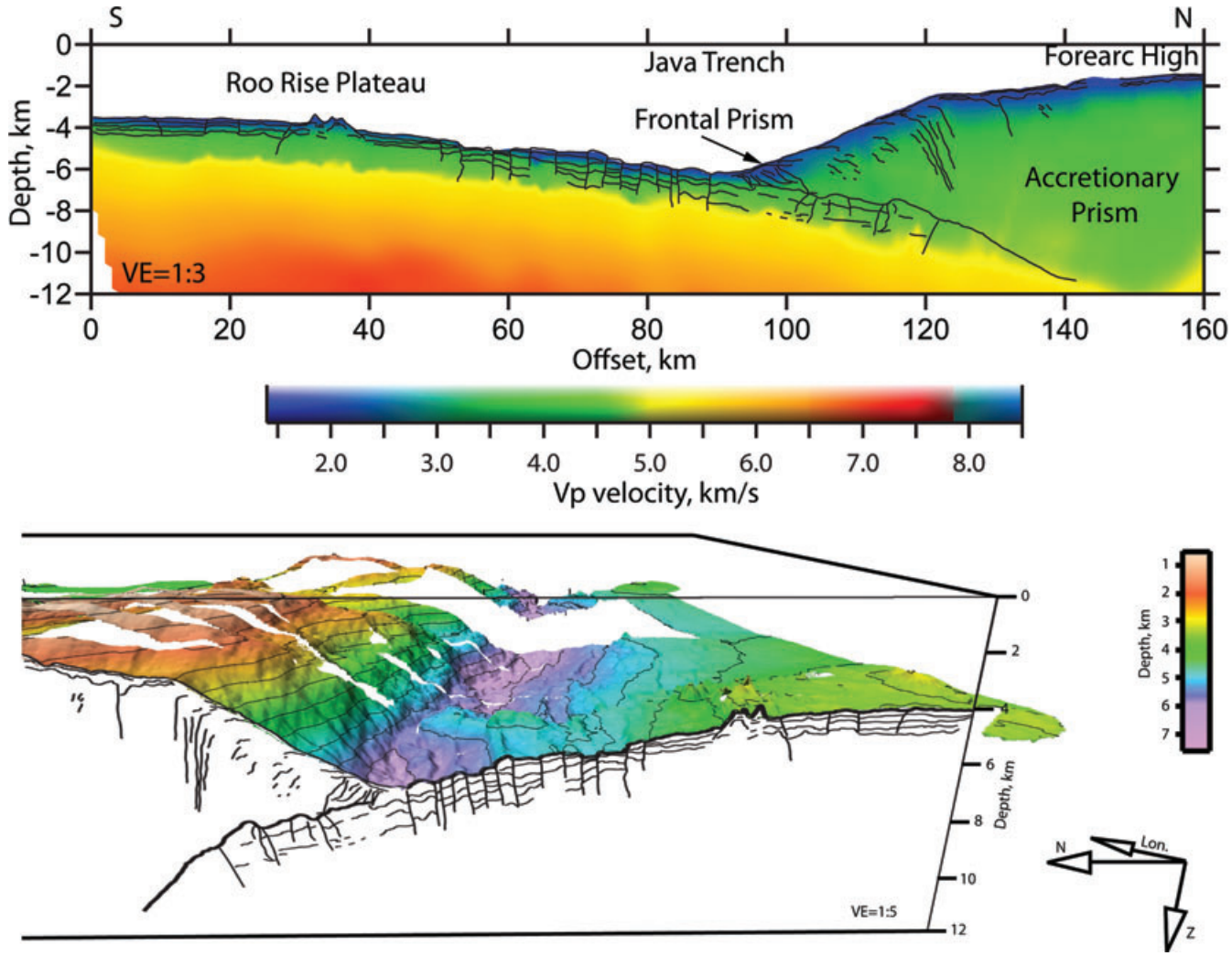

Figure 8. Top panel: A close look on the *Vp* distribution model around the Java trench. The black lines are the line-drawing interpretation of the collocated MCS profile. Bottom panel: 3-D view of the high-resolution bathymetry, centred at the trench location. The view is from west to east. Vertical slice is the linedrawing interpretation of the MCS line collocated with the P4–23 profile. Highly fractured upper oceanic crust is clear visible in both data sets.

Newcomb & McCann (1987) for the presence of a deep crustal root. The observed northward thinning of the Roo Rise crust (Fig. 2) may have several explanations. The most straightforward explanation is to interpret the region with the thinnest crust as the edge of the plateau and its transition to the conventional oceanic crust. Alternatively, this region may represent localized crustal thinning still within the Roo Rise that extends further north. Variations in crustal thickness of up to several kilometres are common for magmatically overprinted oceanic crust and may be associated with past, now inactive, phases of localized increased magmatic activity (Kopp *et al.* 2004). The interpretation of seismicity by Abercrombie *et al.* (2001) suggests the presence of subducted seamounts and thus implies a northward extension of the Roo Rise into the subduction complex. However, as it was shown by the numerical modelling, the presence of a buoyant oceanic plateau subducted below ∼30 km should lead to the formation of a flat subduction and ceasing of magmatism in the volcanic arc (van Hunen *et al.* 2002; Gerya *et al.* 2009; Mason *et al.* 2010). Since it is not the case in this area, we conclude that the main block of the Roo Rise is currently only approaching the trench and the anomalous crustal features present below the forearc are the isolated edge structures of the plateau (i.e. individual seamounts).

Starting from an offset of 60 km further northwards, the oceanic crust is highly fractured and is cut by a number of normal faults clearly visible in the MCS data (Lueschen *et al.* 2010) (Fig. 8) and in the multibeam bathymetry data at the surface (Fig. 1a and b). The observation of the faults and fractures is in an agreement with the results of Masson *et al.* (1990) which show that the subducted oceanic crust is fractured by normal faults due to the tension in its upper part caused by plate bending. Below the trench, the oceanic crust thins to about 10 km and maintains this thickness upon subduction (Fig. 2). The velocities at the top are about 3.5–4.0 km s^{-1} increasing to 5 km s^{-1} at a 2 km depth below see floor, and gradually increasing to 6.5–6.6 km s^{-1} at the Moho. The modelled low velocities are presumably caused by the highly fractured, altered fluid-filled crust which causes the decrease of effective velocities. In addition, velocity smoothing implemented in the tomographic inversion is also likely to contribute to this effect. The lateral variations of the *Vp* velocity structure within the oceanic crust are small (Figs 2 and 8).

Comparison of the obtained structure of the Roo Rise with similar terrains in other regions shows similarities both in the velocity distribution and the crustal thickness. The Hikurangi plateau, offshore New Zealand, which is similar in structure but much larger, is

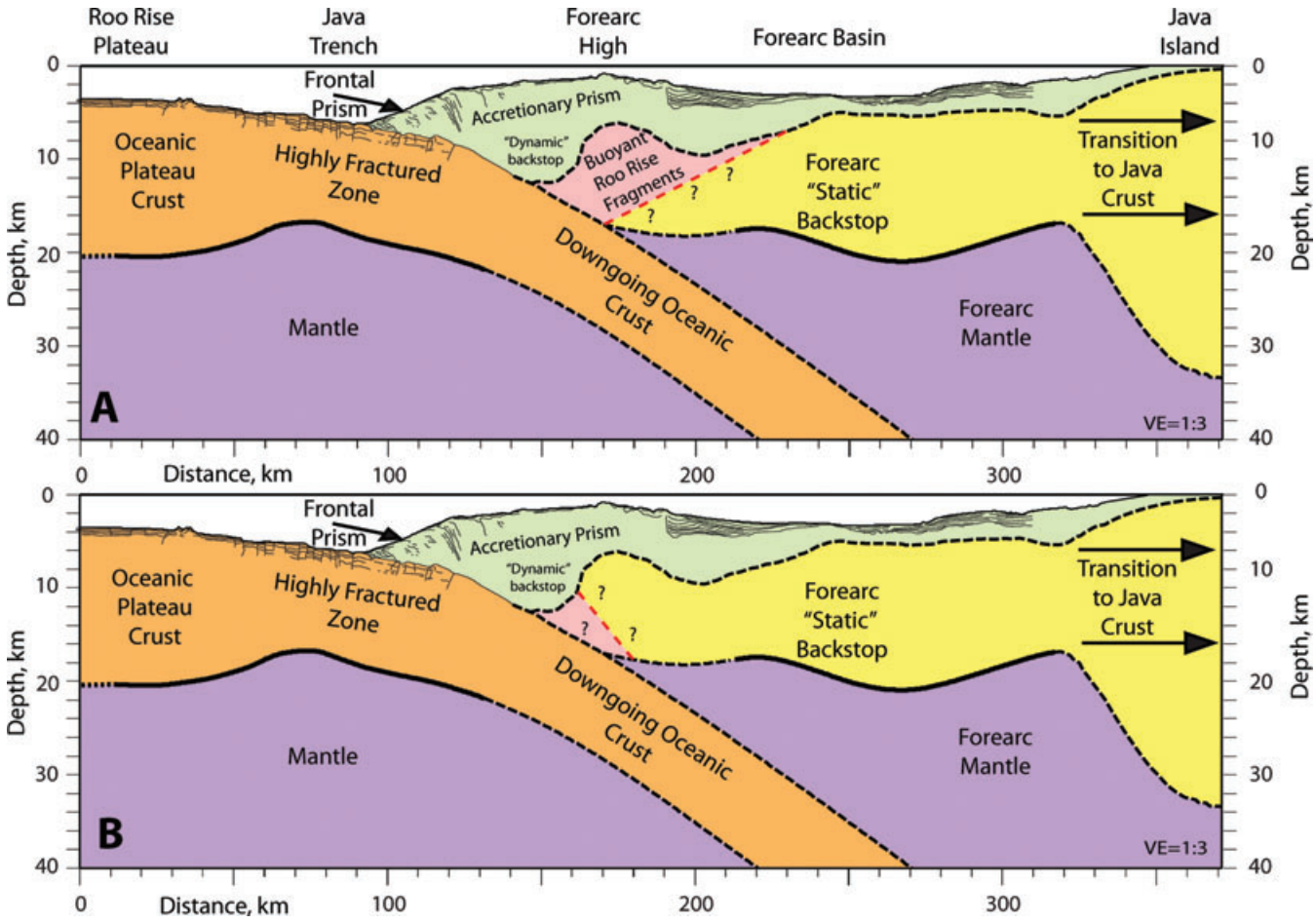

Figure 9. Joint interpretation models for profile P4–23 based on combined results of seismic tomography, MCS and gravity modelling. Thick solid lines are the reflectors constrained by the joint refraction/reflection inversion. Thick dashed lines are structural elements based on the results of gravity modelling. Thin lines are the line-drawing interpretation of the collocated MCS profile. Plots A and B show two variants for the structure of the backstop. (a) Interpretation based on the geometry of the forearc backstop observed to the west from our profile. (b) Interpretation based on the backstop geometry to the east of our profile and the ideas of Bangs *et al.* (2003).

reported to have 10–23-km-thick crust, and *Vp* values ranging from 4.9 to 7.2 km s^{-1} (Davy *et al.* 2008; Scherwath *et al.* 2010). Similar to the Roo Rise, much of the crustal thickening is accommodated by the increase of the lower crust. However, comparing to other Large Igneous Provinces, with common thicknesses of 20–40 km (Coffin & Eldholm 1994), the Roo Rise is at the lower end of these values. This could be due to seismically resolving only the edge of the plateau, but not its centre, where the crust could be thicker. Another comparison could be done with the Nazca ridge offshore Peru, which is more comparable with the size of the Roo Rise, sampled in the study. The crustal thickness of the Nazca ridge reaches 16 km, with *Vp* values ranging from 4.5 to 6.6 km s^{-1} in the upper crust and 6.7 to 7.5 km s^{-1} in the lower crust (Hampel *et al.* 2004). Similar to the Roo Rise and Hikurangi plateaus most of the crustal thickening is accommodated by the lower crust. However, the velocities in the lower crust are much higher compared to the Roo Rise.

3.2 Accretionary prism structure

Starting from the trench (90 km offset) and further north, an active frontal prism is observed, characterized by thrust faults and fronting the accretionary prism (Fig. 8). The frontal prism extends laterally for about 12–15 km. Due to the minor sediment input into the system, the frontal slope of the accretionary prism (from 95 to 125 km offsets) is about 8°–10° with only about 2°–3° in its upper portion, so that the mean slope of ∼5.2° is at the high end of the slope angle range within the neighboring segments (Kopp *et al.* 2006). The frontal prism is characterized by low *Vp* velocity values ranging from 2 to 2.8 km s^{-1}. Further north, in the accretionary prism which extends from 105 to 185 km offsets, velocities increase from 2 km s^{-1} below the sea floor to about 3.5 km s^{-1} at a depth of 3–4 km bsf; the *Vp* velocity in the consolidated sediments in the deeper part of the accretionary prism (6 to 10 km depth) ranges from 3.5 to 5.0 km s^{-1} at the top of the basement.

The accreted sediments forming the forearc high are resolved on both profiles, allowing for a 2.5-D interpretation of this area at the profiles crossing (Fig. 2). The velocity–depth distribution in the sediments is similar for both of the profiles, with *Vp* velocities starting at 2 km s^{-1} and reaching 5 km s^{-1} at the top of the basement at 8 km depth (for the forearc region, we assume the top of the basement to correspond to approximately 5 km s^{-1} isocontour). However, the north–south striking profile suggests a semi-horizontal basement interface extending laterally for, at least, 40 km. This is in contrast to the observations along the east–west profile which reveals a rather undulating topography of the top of the basement, varying from 6 to 10 km depth. This observation can be explained in several ways. It is possible that the forearc crust is composed of several small-scale independent crustal fragments, and thus displays a blocky style of

basement. Another explanation would be to consider the subduction of the basement topographic relief located off profile P4–23, and thus unresolved on it. The presence of such features in the incoming oceanic crust would perturb and dynamically deform not only the overlaying sedimentary packages, but also affect the crustal edge of the backstop.

3.3 Forearc crustal structure

The forearc crust carrying a number of sedimentary basins is located further north, from ∼185 km offset and to the northern termination of the profile (Fig. 2). The depth of the basins ranges from ∼1200 to 1500 m, which is less than in the well-developed forearc basins to the east and to the west where the sediment infill reaches 3 km (Kopp *et al.* 2009a; Planert *et al.* 2010). The *Vp* velocity of the sediment in the basins ranges from 1.7 to 3.0 km s^{-1} in the upper 1–1.5 km (Fig. 2). The velocities in the consolidated sediments above the basement increase from 3.5 to 5.0 km s^{-1}. The crystalline crust of the forearc displays *Vp* velocities ranging from 5.0 km s^{-1} at the top (∼5 km depth) to 6.5–7.0 km s^{-1} at the Moho. The northern segment of the profile (from ∼220 km offset) shows higher velocities in the lower crust, while in between 160 and 220 km offset the velocities in the lower crust do not exceed 6.5 km s^{-1} (Fig. 2). For the same location (∼180 km offset) on the trench-parallel profile, lateral velocity variations in the lower forearc crust are even higher, reaching values up to 7.1 km s^{-1} at 60 km offset of profile P-41 (unfortunately, the low signal-to-noise ratio and a complex 3-D ray propagation for most of the stations on this profile made reflection modelling debatable, especially for the plates interface). The forearc Moho shows minor undulations, as revealed by the tomography model. In the northern section, the Moho is located at a 18 km depth, deepening to ∼20 km at around 270 km offset, and then shallowing again to about 17 km at ∼320 km offset. It indicates that the thickness of the crystalline crust is in the range of 12–16 km. The results from the neighboring segments (111°E and 115°E) image the forearc Moho in a depth range of 14–18 km (Kopp *et al.* 2009b; Planert *et al.* 2010), in agreement with our results. Further to the north, the gravity modelling (Fig. 8) requires a sharp deepening of the Moho to a depth of at least 30 km underneath Java. Crustal deepening can be associated either with the transition to the island arc-like crustal block below Java, or with the presence of the Gondwana revenue as suggested by Smyth *et al.* (2007). Unfortunately, this section is not covered by the seismic data and, due to the non-uniqueness of the gravity modelling, cannot be reliably interpreted.

3.4 Oceanic mantle

The deep structure (below ∼20 km depth) of the profile was resolved mostly in the southern-central portion of the study area (Fig. 2). However, the model resolution is limited for the deep part (Fig. 5). The calculated *Vp* velocity values have an uncertainty of about $-7 + 3$ per cent due to the velocity averaging along the ray paths (Fig. 5). In the uppermost oceanic mantle, the velocities are estimated to be in the range from 7.5 to 7.9 km s^{-1}. The area of the lower seismic velocities is located between 85 and 170 km offset: it starts approximately below the trench and extends to a depth of at least 30 km where the resolution of our model diminishes. The velocities in the forearc mantle are lower as compared to the oceanic mantle; we observe the values of around 7.5–7.6 km s^{-1} under the forearc Moho (Fig. 2). The calculated velocity structure of the forearc and the underlying mantle is in a good agreement with the results calculated for the adjacent segments offshore Lombok and Central Java around 110°E (Kopp *et al.* 2009b; Planert *et al.* 2010).

3.5 Backstop geometry and structure

The backstop edge is located at ∼160 km offset; it represents a near-vertical feature bounding the accretionary prism at depth. The forearc high pattern caused by the Roo Rise approach is unusual, as for the 'normal' oceanic subduction a continuous ridge-like forearc high structure is expected. This should be an effect caused by the oceanic plateau subduction. We speculate on possible scenarios for the structure of the forearc backstop which would explain the observed bathymetry (Fig. 1). Possible options are shown in Fig. 9.

Variant A is based on the geometry of the forearc backstop observed on the profiles to the west from this study, where the backstop gently dips towards the trench (Kopp & Kukowski 2003). The term backstop defines a region within a forearc that is characterized by an increased yield strength compared to the region trenchward of it and thus by its ability to support larger deviatoric stresses. The kinematic discontinuities which form a backstop may be 'static', as would be the case for the continental arc basement, or 'dynamic' and thus still deforming, though at a slow rate, as may be expected for compacted accreted material resulting from an earlier phase of accretion (Kopp & Kukowski 2003). In the latter case, the material located southward of the 'static' backstop would represent buoyant fragments of the oceanic plate, of the Roo Rise nature, which were detached from the plate and stacked over the static backstop (i.e. little-deforming continental arc basement, following Kopp & Kukowski (2003)). This scenario is valid under conditions that the oceanic crust, currently subducted below the accretionary complex, was as fractured as the segment currently observed at around trench, and that there were some elevated relief features that would have detached from the plate. In this case, the observed forearc high would correspond to the area of maximum stacking of such relief revenues against the static forearc backstop. This correlates with the location of the forearc highs and also explains the relatively shallow forearc basins, as they would experience uplift together with a lateral compression.

Variant B is based on the similarities of our study region to the Lesser Antilles subduction zone. The subduction of the large aseismic Tiburon ridge might be comparable by size and scale to the subduction of the Roo Rise. Following this analogy and the ideas of Bangs *et al.* (2003) and Christeson *et al.* (2003), we speculate on the other option for the backstop structure (Fig. 9b). In this case, the static forearc backstop geometry is similar to the one observed on the profile located eastwards from the study area, offshore Lombok (Planert *et al.* 2010). The observed forearc high then would be linked to the bending-related uplift of the forearc edge, caused by the presence of stacked fragments of the oceanic origin below it. The same conditions should be valid for this scenario as in option A. For this case, the location of the forearc high and its uplift are correlated with the uplift of the crystalline forearc edge.

The choice of any particular variant is governed by the geometry of the static forearc backstop at its exact location, which is not resolved in the study. However, both of the options would influence the geohazard potential for the area, including tsunami and earthquakes. The detailed assessment of the geohazards is outside of the scope of this study. Following, will provide some insight on the earthquake and tsunami potential of the region. In order to trigger a tsunami, a sufficient vertical movement of the seafloor is required. This can be achieved either by crustal movements on the

trust faults as a result of earthquake slip, or as a result of a submarine landslide, possibly triggered by an earthquake. The 2004 Sumatra earthquake and tsunami is an example of the large mega-thrust event where the major slip was accommodated on the trust faults, resulting in ∼14 m uplift (Sibuet *et al.* 2007). Similar settings are expected for the Chili and the Cascadia margins. The submarine landslides are the explanation for the tsunamis in the Atlantic region and other regions such as Papua New Guinea and Puerto Rico (ten Brink *et al.* 2009), which puts them into a special class of geohazard as the initiating earthquakes can be much smaller than in mega-thrust events. Offshore Java, where the frontal erosion causes the oversteepening of the frontal slope, any changes in the seismicity regime are of high importance. Both proposed crustal interpretations invoke local deformation of the backstop and the overlaying sediments and can lead to the formation of large laterally inhomogeneous stress gradients in the area, thus increasing the probability of rupture on the normal faults in the oceanic crust due to load as well as on thrust faults within the accretionary prism and within the seismogenic zone. It explains the observed increased level of the shallow seismicity clustered around 113°E (Fig. 1) and the dynamically caused perturbations of the basement top and associated forearc high. A similar seismicity pattern is observed in the Lesser Antilles subduction zone where the clustering of shallow seismicity is spatially correlated with the collision of the subducting aseismic ridge with the backstop (Christeson *et al.* 2003). Unfortunately, the lack of deep penetrating seismic reflection data imaging the internal structure of the observed crustal edge and the absence of local relocated seismicity leaves this question open for further research.

The northward shift of the active volcanic arc observed on Java (Fig. 1) can be correlated to the northward trench r advancing in the vicinity of the Roo Rise, approaching the trench. The presence of elevated bathymetric features associated with sea plateau subduction can cause the frontal erosion of the accretionary complex and thus the landward migration on the trench. Numerical modelling shows that it can be considered as an initial stage of the formation of a flat shallow subduction and ceasing of melt production (van Hunen *et al.* 2002; Gerya *et al.* 2009). Furthermore, a proposed Gondwana revenue (Smyth *et al.*, 2007), located in between the trench and Southern Java, can be also responsible for producing complex interaction processes within the subduction system, resulting in the northward volcanic arc propagation. The structure of this lithospheric block and the processes that it triggers are unclear and should be studied in order to understand the entire dynamics of this subduction margin.

Summarizing, we observe the complex subduction of abnormally thick oceanic crust under the rigid forearc crust. The accretionary complex is experiencing an inhomogeneous current uplift due to one of the proposed scenarios. The approach of the buoyant oceanic plateau to the trench causes active frontal erosion as well as internal deformation of the accreted sediments which, in turn, dynamically affects the tip of the forearc crust and the structure of the forearc basins. This complex deformation pattern has a strong effect on local seismicity and increases the geohazard risk for tsunamogenic seismic events.

4 CONCLUSION

The summary of our results is shown in Fig. 9. In the 113°E segment of the Java trench, we observe the approach of the oceanic plateau Roo Rise to the trench, and the effects it causes on the local subduction regime.

The Roo Rise is characterized by variable crustal thickness ranging from 18 to 12 km and shallowing towards Java. It extends laterally for at least 70 km within our profile (Fig. 2). Based on the bathymetric data and its link to the presence of a deep compensating crustal root, the thickened oceanic plateau crust with an average thickness of about 15 km is expected to cover an area of approximately 100 000 km^2 (200 km × 500 km) offshore Central-Eastern Java. The transition to normal oceanic crust is not well defined, but the plateau can extend into the subduction system up to 60 km northward from the trench.

The structure of the upper crust of the incoming oceanic plate shows a high degree of fracturing in its top section. This fracturing is clearly visible in the high-resolution bathymetry and MCS transect down to 2 km below the top of the crust (Fig. 8). It is possible that the crust is cut by faults even to a greater depth, as indicated by the low mantle velocities that require fluid percolation (Carlson & Miller 2003), and by an increased level of shallow crustal seismicity (Abercrombie *et al.* 2001; Bilek & Engdahl 2007).

Within our profiles, we do not recover any direct evidence for the presence of the bathymetric features on the oceanic plate currently present below the accretionary prism. Depth variations of the basement observed on the trench-parallel profile, may serve as evidence for bathymetric features associated to the RooRise.

Gravity modelling requires a sharp crustal thickness increase below Java. As the region is not covered with seismic data, we can only speculate on the origin of this crustal structure. The thick crust can be a part of the Gondwana revenue as suggested by Smyth *et al.* (2007).

The approach of the Roo Rise to the trench has strong effects on the local seismicity setting. The geohazard risks should be reconsidered as this segment of the margin has an increased probability for tsunamogenic earthquakes.

ACKNOWLEDGMENTS

We would like to thank Cpt. Meyer and the crew of R/V Sonne and the SINDBAD Working group for their enormous help in collecting and processing of the data. We express great gratitude to Jun Korenaga for the discussion of seismic tomography and the Tomo2D code. We highly appreciate the reviews and comments from Saskia Goes and Gail Christeson, which improved the paper. We would like to extend special thanks to Greg Houseman and Alessandro Forte for fruitful discussions. The SINDBAD project is funded by the German Federal Ministry of Education and Research (BMBF) (grants 03G0190A and 03G0190B). Special thanks to Petersen-Stiftung foundation for their funding to complete this study.

REFERENCES

Abercrombie, R., Antolik, M., Felzer, K. & Ekström, G., 2001. The 1994 Java tsunami earthquake: slip over a subducting seamount, *J. geophys. Res.,* **106,** 6595–6607.

Bangs, N.L., Christeson, G.L. & Shipley, T.H., 2003. Structure of the Lesser Antilles subduction zone backstop and its role in a large accretionary system, *J. geophys. Res.,* **108**(B7), doi:10.1029/2002JB002040.

Bialas, J. & Flueh, E.R., 1999. Ocean bottom seismometers, *Sea Technol.,* **40**(4), 41–46.

Bilek, S.L. & Engdahl, E.R., 2007. Rupture characterization and aftershock relocations for the 1994 and 2006 tsunami earthquakes in the Java subduction zone, *Geophys. Res. Lett.,* **34,** L20311.

Carlson, R.L. & Herrick, C.N., 1990. Densities and porosities in the oceanic crust and their variations with depth and age, *J. geophys. Res.,* **95,** 9153–9170.

Carlson, R.L. & Miller, D.J., 2003. Mantle wedge water contents estimated from seismic velocities in partially serpentinized peridotites, *Geophys. Res. Lett.,* **30**(5), 1250, doi:10.1029/2002GL016600.

Christensen, N.I. & Mooney, W.D., 1995. Seismic velocity structure and composition of the continental crust: a global view, *J. geophys. Res.,* **100,** 9761–9788.

Christeson, G.L., Bangs, N.L. & Shipley, T.H., 2003. Deep structure of an island arc backstop, Lesser Antilles subduction zone, *J. geophys. Res.,* **108**(B7), doi:10.1029/2002JB002243.

Coffin, M.F. & Eldholm, O., 1994. Large igneous provinces: crustal structure, dimensions, and external consequences, *Rev. Geophys.,* **32**(1), 1–36, doi:10.1029/93RG02508.

Curray, J.R., Shor, G.G., Rait, R.W. & Henry, W., 1977. Seismic refraction and reflection studies of crustal structure of the eastern Sunda and western Banda Arcs, *J. geophys. Res.,* **82,** 2479–2493.

Davy, B., Hoernle, K. & Werner, R., 2008. Hikurangi Plateau: crustal structure, rifted formation, and Gondwana subduction history, *Geochem. Geophys. Geosyst.,* **9,** Q07004, doi:10.1029/2007GC001855.

DeMets, C., Gordon, R.G., Argus, D.F. & Stein, S., 1994. Effect of recent revisions to the geomagnetic reversal time-scale on estimates of current plate motions, *Geophys. Res. Lett.,* **21**(20), 2191–2194.

Gerya, T.V., Fossati, D., Cantieni, C. & Seward, D., 2009. Dynamic effects of the aseismic ridge subduction: numerical modeling, *Eur. J. Mineral.,* **21**(3), 649–661.

Hall, R., 2002. Cenozoic geological and plate tectonic evolution of SE Asia and the SW Pacific: computer-based reconstructions, model and animations, *J. Asian Earth Sci.,* **20,** 353–434.

Hall, R. & Smyth, H.R., 2008. Cenozoic arc processes in Indonesia: identification of the key influences on the stratigraphic record in active volcanic arcs, *Geol. Soc. Am. Spec. Pap.,* **436,** 27–54.

Hamilton, W., 1979. Tectonics of the Indonesian region. *U. S. Geol. Surv. Prof. Pap.,* **1078,** 308–335.

Hamilton, W., 1988. Plate tectonics and island arcs, *Geol. Soc. Amer. Bull.,* **100,** 1503–1527.

Hampel, A., Kukowski, N., Bialas, J., Hebscher, C. & Heinbockel, R., 2004. Ridge subduction at an erosive margin: the collision zone of the Nazca Ridge in southern Peru, *J. geophys. Res.,* **109,** B02101, doi:10.1029/2003JB002593

Kopp, H. & Kukowski, N., 2003. Backstop geometry and accretionary mechanics of the Sunda Margin, *Tectonics,* **22**(6), 1072, doi:10.1029/2002TC001420.

Kopp, H. *et al*. 2009b. *Convergent Margin Structure and Tectonics of the Java Subduction Zone (105°E-122°E), EOS,* Vol. 90, Number 52, 29 December 2009, Fall Meet. Suppl. Abstract T33B-1916.

Kopp, H., Flueh, E.R., Klaeschen, D., Bialas, J. & Reichert, C., 2001. Crustal structure of the central Sunda margin at the onset of oblique subduction, *Geophys. J. Int.,* **147,** 449–474.

Kopp, H., Flueh, E.R., Papenberg, C. & Klaeschen, D., 2004. Seismic investigations of the O'Higgins Seamount Group and Juan Fernandez Ridge: aseismic ridge emplacement and lithosphere hydration, *Tectonics,* **23,** TC2009, doi:10.1029/2003TC001590.

Kopp, H., Flueh, E.R., Petersen, C.J., Weinrebe, W., Wittwer, A. & Meramex Scientists., 2006. The Java margin revisited: evidence for subduction erosion off Java, *Earth planet. Sci. Lett.,* **242,** 130–142.

Kopp, H., Hindle, D., Klaeschen, D., Oncken, O. & Scholl, D., 2009a. Anatomy of the western Java plate interface from depth-migrated seismic images, *Earth planet. Sci. Lett.,* doi:10.1016/j.epsl.2009.09.043.

Kopp, H., Klaeschen, D., Flueh, E.R. & Bialas, J., 2002. Crustal structure of the Java margin from seismic wide-angle and multichannel reflection data, *J. geophys. Res.,* **197**(B2), doi:10.1029/2000JB000095.

Korenaga, J., Holbrook, S., Kent, G., Kelemen, P., Detrick, R.S., Larsen, H.-C., Hopper, J.R. & Dahl-Jensen, T., 2000. Crustal structure of the southeast Greenland margin from joint refraction and reflection seismic tomography, *J. geophys. Res.,* **105,** doi:10.1029/2000JB900188.

Lueschen, E., Mueller, C., Kopp, H., Engels, M., Lutz, R., Planert, L., Shulgin, A. & Djajadihardja Y., 2010. Structure, evolution and tectonic activity at the Eastern Sunda forearc, Indonesia, from marine seismic investigations, *Tectonophysics,* in press, doi:10.1016/j.tecto.2010.06.008.

Mason, W.G., Moresi, L., Betts, P.G. & Miller, M.S., 2010. Three-dimentional numerical models of the influence of a buoyant oceanic plateau on the subduction zones, *Tectonophysics,* **483,** doi:10.1016/j.tecto.2009.08.021.

Masson, D.G., 1991. Fault patterns at outer trench walls, *Mar. geophys Res.,* **13,** 209–225.

Masson, D.G., Parson, L.M., Milsom, J., Nichols, G., Sikumbang, N., Dwiyanto, B. & Kallagher, H., 1990. Subduction of seamounts at the Java Trench: a view with long-range sidescan sonar, *Tectonophysics,* **185,** 51–65.

Moore, G.F., Curray, J.R., Moore, D.G & Karig, D.E., 1980. Variations in geologic structure along the Sunda Fore Arc, northeastern Indian Ocean, in *The Tectonic and Geologic Evolution of Southeast Asian Seas and Islands,* Vol. **23**, pp. 145–160, eds Hays, D.E., Geoph. Mon.

Mueller, C. *et al*. 2008. From subduction to collision: the Sumba-Banda Arc transition, *EOS, Trans. Am. geophys. Un.,* **89,** 49–50.

Newcomb, K.R. & McCann, W.R., 1987. Seismic history and seismotectonics of the Sunda Arc, *J. geophys. Res.,* **92**(B1), 421–439.

Planert, L., Kopp, H., Lueschen, E., Mueller, C., Flueh, E.R., Shulgin, A., Djajadiharja, Y. & Krabbenhoeft, A., 2010. Lower plate structure and upper plate deformational segmentation at the Sunda-Banda arc transition, *J. geophys. Res.,* **115,** B08107, doi:10.1029/2009JB006713.

Scherwath, M. *et al*. 2010. Fore-arc deformation und underplating at the northern Hikurangi margin, New Zealand, *J. Geol. Res.* **115,** B06408, doi:10.1029/2009JB006645.

Scholz, C.H. & Small, C., 1997. The effect of seamount subduction on seismic coupling, *Geology,* **25,** 487–490.

Shulgin, A. *et al*. 2009. Sunda-Banda arc transition: incipient continent-island arc collision (northwest Australia), *Geophys. Res. Lett.,* **36,** L10304, doi:10.1029/2009GL037533.

Sibuet, J-C. *et al*. 2007. 26th December 2004 great Sumatra-Adamant earthquake: co-seismic and post-seismic motions in northern Sumatra, *Earth planet. Sci. Lett.,* **263,** doi:10.1016/j.epsl.2007.09.005.

Smyth, H.R., Hamilton, P.J., Hall, R. & Kinny, P.D., 2007. The deep crust beneath island arcs: inherited zircons reveal a Gondwana continental fragment beneath East Java, Indonesia, *Earth planet. Sci. Lett.,* **258,** 269–282.

ten Brink, U.S., Lee, H.J., Geist, E.L. & Twichell, D., 2009. Assesment of tsunami hazard to the U.S. East Coast using relationships between submarine landslides and earthquakes, *Mar. Geol.,* **264,** doi:10.1016/j.margeo.2008.05.011.

Tregoning, P. *et al*. 1994. First geodetic measurement of convergence across the Java Trench, *Geophys. Res. Lett.,* **21**(19), 2135–2138.

van Hunen, J., van den Berg, A.P. & Vlaar, N.J., 2002. On the role of subducting oceanic plateaus in the development of shallow flat subduction, *Tectonophysics,* **352,** 317–333.

Werner, R., Hauff, F. & Hoernle, K., 2009. RV Sonne. Cruise report SO-199 CHRISP. Christmas Island Seamount Province and the Investigator Ridge: age and causes of intraplate volcanism and geodynamic evolution of the south-eastern Indian ocean, **25,** 1614–6298.

White, R.S., McKenzie, D. & O'Nions, R.K., 1992. Oceanic crustal thickness from seismic measurements and rare earth element inversions, *J. geophys. Res.,* **97,** 19 681–19 715.

Wiener, N., 1949. *Extrapolation, Interpolation, and Smoothing of Stationary Time Series,* John Wiley and Sons, New York.

Yamazaki, T. & Okamura, Y., 1989. Subducting seamounts and deformation of overriding forearc wedges around Japan, *Tectonophysics,* **160,** 207–229.

SUPPORTING INFORMATION

Additional Supporting Information may be found in the online version of this article:

Figure S1. The comparison of all the picked traveltimes available for the tomographic inversion for the two profiles. The picked traveltimes are shown by black dots for the refracted phases and green dots for the reflected phases. Corresponding computed traveltimes through our final models are shown by red and blue dots, for the refracted and reflected phases, respectfully. Top plot is the fit comparison for the N–S profile, bottom—for the E–W profile. Note, the identical distance and timescale for both plots.

Please note: Wiley-Blackwell are not responsible for the content or functionality of any supporting materials supplied by the authors. Any queries (other than missing material) should be directed to the corresponding author for the article.